A study of velocity discontinuity for single air bubbles rising in an associative polymer

E. Soto, C. Goujon, R. Zenit, and O. Manero
*Instituto de Investigaciones en Materiales Universidad Nacional Autónoma de México,
Apdo. Postal 70-360, México D.F. 04510, México*

The motion of air bubbles in aqueous solutions of a hydrophobic alkali-swellable associative polymer is studied in this work. The associative nature of these polymer systems dictates their rheological properties: for moderate values of the shear rate, the formation of structure can lead to a shear-thickening behavior and to the appearance of first normal stress difference. For larger shear rates, the polymer associations can be broken, leading to shear thinning. In general, these fluids show a Newtonian behavior for small values of the shear rate, but behave as viscoelastic liquids for large shear rates. Experimental results show the appearance of a critical bubble volume at which a discontinuity in the relation velocity-volume occurs; however, the velocity increase found in this case is not as large as that previously reported for the case of shear-thinning viscoelastic fluids. The discontinuity is associated with a significant change of the bubble shape: before the critical volume, the bubbles are convex spheroids, while past the critical volume a sharp cusped end appears. The appearance of the tail is also associated with the appearance of an inflection point (change of curvature) on the bubble surface. Moreover, since the rheology of the liquids is measured it was found that the discontinuity, and hence the change of shape, occurs when the elastic nature of the liquid first manifests itself (appearance of a first normal stress difference). A comparison of the measured velocities for small bubbles with predictions from a Stokes-Hadamard law shows a discrepancy. The Newtonian viscosity measured in a viscometric flow was smaller than that determined from a falling-ball arrangement. Considering the viscosity measured under this nonviscometric flow, the comparison between theory and experiments was very good for bubbles having volumes lower than the critical one. Moreover, due to the importance of the elasticity, and due to the change of the shape of the bubble, a dimensionless number formed as the ratio of elastic to surface tension forces clearly defines the change of the behavior for the bubbles rising in these fluids. Finally, a photographic study of the peculiar shapes of the bubble tails, tip-, and *edge*-streaming phenomena is presented. To our knowledge, experiments in this class of fluids have not been reported to date. © *2006 American Institute of Physics*. [DOI: 10.1063/1.2397011]

I. INTRODUCTION

The study of the motion of air bubbles in liquids has received much attention because of its fundamental and practical importance. For the case of Newtonian liquids, there is a vast collection of investigations that report interesting behaviors in many regimes.[1] The understanding of such a system is quite complete. For the case of the motion of gas bubbles in non-Newtonian liquids, there are several unexpected phenomena that remain to be fully understood.[2,3]

Among the peculiar phenomena observed in the case of non-Newtonian liquids, of particular interest is the so-called *bubble velocity discontinuity*. In a Newtonian fluid, the magnitude of the rising velocity of a gas bubble is proportional to the bubble size and the relation velocity-volume is monotonically increasing. For the case of non-Newtonian liquids, many authors[4–10] have reported that there exists a critical value of the volume of the bubble for which a discontinuity of the velocity occurs: the bubble velocity increases monotonically as the bubble size increases, but once a critical volume is reached, the bubble velocity increases in a discontinuous manner. In other words, the bubble velocity can increase many times for a slight increase of the bubble volume. Astarita and Apuzzo[4] were the first to report that the ratio of the velocity after and before the jump ranged from 2 to 6, depending on the polymer present in the solution. They argued that this discontinuity of the velocity was a result of a transition from the Stokes regime to the Hadamard regime (a change from a rigid to a free interface). However, it can be shown that the velocity increase resulting from such a change of the boundary conditions would be equal to 1.5. Due to the fact that no discontinuity of the velocity has been reported to occur for the case of falling spheres, some authors[5–7] have supported this argument, even though it does not predict correctly the increase of velocity. Astarita and Apuzzo[4] also pointed out that the shape of the bubbles changed before and after the velocity discontinuity.

Rodrigue *et al.*[8] proposed an explanation for the discontinuity. They argued that it results from a balance between elastic and Marangoni instabilities, providing another major difference between Newtonian and non-Newtonian hydrodynamics. They have also studied the effect of surfactants in the liquid,[9] and concluded that surface active agents as well

18, 121510-1

as elastic forces must be simultaneously present in order to generate a sudden jump in velocity.

Recently, Herrera-Velarde *et al.*[10] studied the velocity field around bubbles before and after the critical volume by means of a particle image velocimetry (PIV) technique. They reported that the appearance of the velocity discontinuity is associated with the presence of the so-called *negative wake*: for small bubbles (with a volume smaller than the critical volume) the flow is similar to that of a bubble moving in a Newtonian liquid; for large bubbles (with a volume larger than the critical volume), the flow is strongly different and a negative wake is present. The wake is called "negative" because the velocity, very close to the trailing end, is in the direction of the motion of the bubbles; a short distance away from the trailing end, the velocity reverses direction. For a bubble rising in a Newtonian liquid, the wake is normal, as the velocity in the wake is in the same direction as the motion of the bubble. Hassagar[11] was the first to observe this behavior for bubbles and coined the term "negative wake." Negative wakes have also been observed for spheres falling in viscoelastic liquids.[12] Many explanations have been proposed to explain the appearance of this discontinuity; however, a complete self-consistent explanation is not yet available.

In order to acquire certain desired rheological characteristics in commercial products, rheology modifiers are used, i.e., surfactants (worm-like micellar systems), polymers (cellulose derivates), and hydrophobically modified or associative polymers (hydrophobically modified hydroxyethylcellulose).[15,16] In particular, surfactants and associative polymers are formed by two main parts: one hydrophobic and the other hydrophilic. In aqueous solutions, the hydrophilic part is surrounded by water while the hydrophobic parts associate themselves with forming agglomerates called micelles. The formation and rupture of these structures dictate the rheological behavior of these solutions. In general, for associative polymers and surfactants, modifications of rheological properties can be accomplished with smaller concentrations, compared to those needed for ordinary polymers, hence reducing the amount of residual products.

In this investigation, experiments to determine the terminal velocity of air bubbles in solutions of a hydrophobically modified alkali soluble polymer (HASE) were conducted. HASE is an associative polymer formed by a hydrophilic principal backbone and some pendant hydrophobic groups in a comb-like arrangement.[15,16] HASE solutions display complex rheological properties because they exhibit a shear thickening and/or thinning in addition to viscoelasticity. At some specific concentrations HASE solutions have a region of constant viscosity, but with the presence of elasticity, it is possible to isolate elastic and shear-thinning effects. Another advantage of using these liquids is that they serve as model systems.[17,18]

To our knowledge, experiments to determine terminal velocities of gas bubbles on HASE-type fluids have not been reported to date. Belmonte[19] reported experimental results of gas bubbles rising in worm-like micellar liquids, which share a similar complex rheology as the HASE system presented here. For these solutions, the bubbles develop a cusped edge
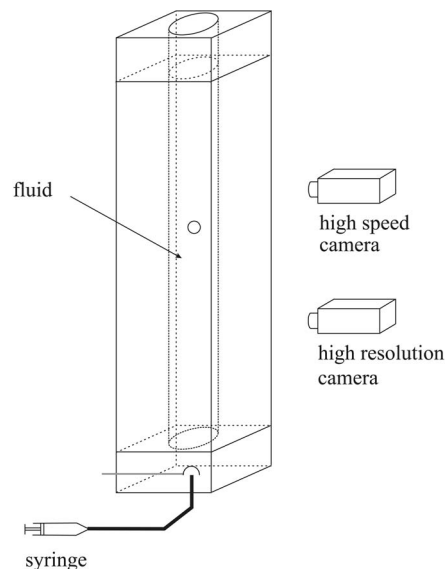

FIG. 1. Experimental device to study the motion of air bubbles in a liquid. Two cameras (one high speed and one high resolution) allow us to determine the velocity and shape of the bubble.

and, for some conditions, self-trajectory oscillations appeared. Some authors[20–22] reported that the motion of settling spheres in micellar-type fluids also shows trajectory oscillations.

In this paper, we present experimental results for single bubbles rising in a HASE associative polymer. In Sec. II, the experimental methods are presented. The theory concerning bubbles moving in a Newtonian liquid at low Re is briefly summarized (Sec. III). After presenting the experimental results (Sec. IV) and their comparison with the theory (Sec. V), we present an explanation of the discontinuity of the velocity based on the rheological properties of the liquid. In the last section (Sec. VI), we present a short study of the shape of bubble tails that appears after the discontinuity.

II. EXPERIMENTAL METHODS

A. Materials and experimental setup

To analyze the motion of air bubbles in a liquid, the experimental device, presented in Fig. 1, was used. A certain volume was placed in a cap with a syringe, and by turning the cap, the bubble was released to move upwards in the inner tube. The width of the inner tube ($D=9$ cm) was enough to minimize wall effects. In all cases, the ratio between the diameter of the bubble and the diameter of the inner tube was smaller than 0.1. The inner tube length ($L=60$ cm) was long enough for the bubbles to reach a stable terminal velocity. In the outer square tube, a liquid with the same refraction index as the solution present in the inner tube was placed to reduce the refraction effects. Several HASE concentrations were tested and their rheological characterization is presented in the next part. Since, it has been shown that the velocity of the bubbles can be dependent on the injection frequency,[9] a 5-min interval was left between two consecutive bubbles to avoid this effect.

TABLE I. Properties of the bubbles (diameter d and equivalent shear rate $\dot{\gamma}=U/r$) in different solutions.

Fluid $n°$	% HASE	d (mm)	$\dot{\gamma}$ (s^{-1})
1	1.2%	0.3–9.4	1–42
2	1.5%	3.3–7.6	2–16
3	1.7%	2.5–8.7	1–10

TABLE II. Properties of the solutions: viscosity μ, surface tension σ, and coefficients a and b in the expression of the first normal stress difference, $N_1 = a\dot{\gamma}^b$.

Fluid $n°$	% HASE	μ (Pa s)	σ (mN m)	a	b	Range of $\dot{\gamma}$
1	1.2%	0.22±0.009	38.41±0.34	0.2078	1.3097	0.1–100
2	1.5%	1.14±0.005	36.93±0.23	1.1449	1.3192	0.1–100
3	1.7%	3.34±0.04	55.55±0.38	2.3728	1.3289	0.1–50

HASE (Primal TT-935) is supplied by Rohm and Haas. Aqueous solutions were prepared at 1.2, 1.5, and 1.7% by weight in distilled water and left to rest for 48 h. A 0.5-M solution of 2-amino,2-methyl propanol (AMP), supplied by Aldrich, was used to adjust the pH to 9.0, at which the viscosity is a function of pH peaks. Once the solutions were free of bubbles, the rheological and surface tension properties were determined.

B. Measurement methods

1. Bubble shape and velocity

The bubble terminal velocity and shape were determined using two cameras. The first one was a high-speed camera (RedLake MotionScope Model 1000), which measures the velocity of the bubble using spatiotemporal diagrams. The error in the bubble velocity determination was smaller than 1.5 mm/s. The second one was a high-resolution camera (6 megapixels, Fuji FinePix S1pro), which determines the bubble's geometric characteristics (shape and volume) by image analysis. The bubble volume was determined assuming axial symmetry. Comparing the value of a known injected volume with that obtained by image analysis, the error is smaller than 2%. An average shear rate $\dot{\gamma}$ was defined to characterize the rheological properties of the fluid as the ratio of the terminal velocity U of the bubble to its spherical equivalent radius r: $\dot{\gamma}=U/r$. As shown elsewhere, the mean value of the shear rate $\dot{\gamma}$ can be given by U/r for the flow
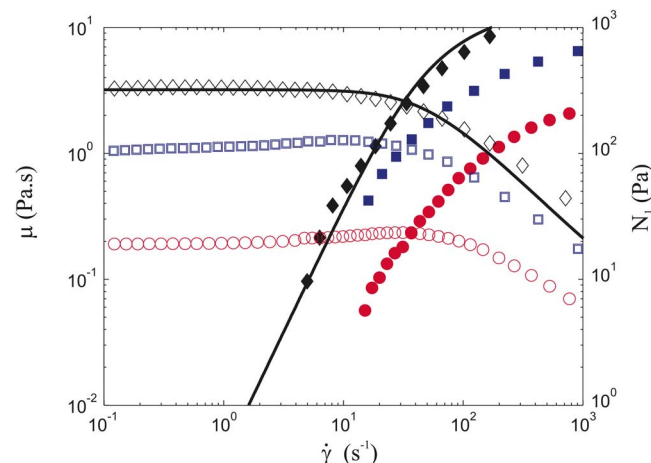
around a spherical bubble at low Reynolds number.[23,24] The experimental range of the bubbles diameter and mean shear rates are presented in Table I.

The flow field around the bubble on the symmetry plane was determined using PIV, with a commercial device provided by Dantec Dynamics. The light source was a 532-nm laser; fluorescent seeding and filters were used to avoid reflections within the air-liquid interface. More details about this technique can be found in Ref. 10.

2. Rheological properties

The rheological properties of the HASE solutions under simple shear were determined in a stress-controlled rheometer (TA Instruments), using a 40-mm $1°59'$ cone and plate fixture with a Peltier temperature-control system.

The HASE solutions tested behave as Newtonian fluids (at small shear rates, viscosity remains constant and normal stresses are negligible; Fig. 2). From 0.1 to 50 s^{-1}, the normal stresses are measurable while the viscosity remains almost constant. For all concentrations, a slight shear-thickening behavior can be observed for small ranges of shear rate (for 1.2% HASE, $6<\dot{\gamma}<36$; for 1.5% HASE, $2<\dot{\gamma}<12$; for 1.7% HASE, $1<\dot{\gamma}<3.7$). For large shear rates and depending on the concentration, the fluids exhibit a shear-thinning behavior: the viscosity decreases with the
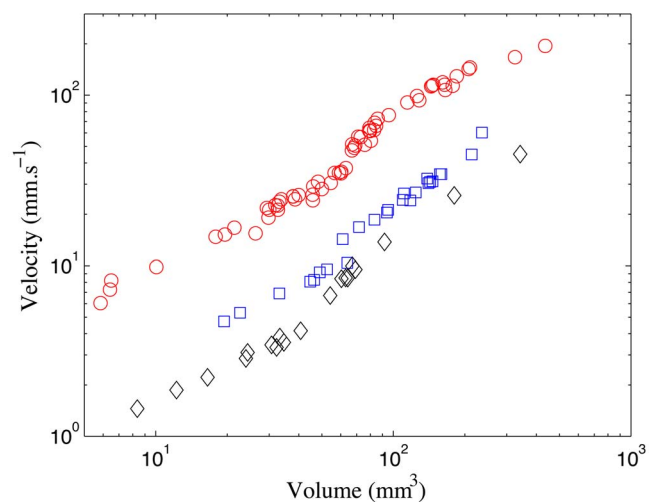

FIG. 2. Shear viscosity μ (empty symbols) and first normal stress difference N_1 (solid symbols) as a function of the shear rate for different percentages of HASE (∘) 1.2%; (□) 1.5%; (◇) 1.7%. The bold lines show predictions of the Bautista-Manero model for 1.7% of HASE (Ref. 18).

FIG. 3. Bubble velocity as a function of bubble volume for different percentages of HASE: (∘) 1.2%; (□) 1.5%; (◇) 1.7%. There is a discontinuity of the bubble velocity for volumes equal to V_c (1.2%: $V_c \simeq 65$ mm^3; 1.5%: $V_c \simeq 60$ mm^3; 1.7%: $V_c \simeq 50$ mm^3). The critical volume decreases with an increase in HASE concentration.

shear rate and the first normal stress difference increases with the shear rate. In general, for a given shear rate, the viscosity and the first normal stress difference increase with HASE concentration, and the critical value of the shear rate at which normal stresses appear decreases with increasing HASE concentration.

For the first normal stress difference, it is possible to fit the data to a power law, $N_1 = a\dot{\gamma}^b$. The coefficients a and b, and the range of shear rate for which this assumption is valid, are reported in Table II. The predictions of the model by Bautista *et al.*[18] are shown with experimental data for the 1.7% HASE solution (Fig. 2). As analyzed elsewhere,[25] this model accounts for the breakage-reformation process of the structure of associative polymers under flow. The model predicts a maximum in the extensional viscosity at a strain rate corresponding to that of the onset of normal stresses and the shear-thinning region of the shear viscosity.

The surface tension of these liquids was measured with a Wilhelmy balance (Sigma 700) using a DuNouy ring (Table II).

$$C_d = \begin{cases} 24/\mathrm{Re}, & \text{rigid interface,} & \text{Stokes drag} \\ 16/\mathrm{Re}, & \text{free interface,} & \text{Hadamard-Rybczynski drag} \end{cases}.$$

Hence, the terminal velocity for each case is

$$U_{\text{Stokes}} = \frac{\rho g}{18\mu} d^2, \tag{1}$$

$$U_{\text{Hadamard}} = \frac{\rho g}{12\mu} d^2, \tag{2}$$

where d is the equivalent diameter of the bubbles (m), ρ is the density of the liquid (kg m^{-3}), g is the gravitational constant ($g = 9.81$ ms^{-2}), and μ is the viscosity of the liquid (Pa s).

In the case of very small bubbles rising in the HASE solution, the shear rate is very small, and then the liquid can be considered as Newtonian: there are no normal stresses and the viscosity is constant. However, it is very difficult to determine the surface boundary condition (rigid or free). As an example, a "dirty" bubble will not have a free or a rigid interface; hence, one would expect to observe a behavior between the two regimes.

IV. EXPERIMENTAL RESULTS

A. Bubble terminal velocity and velocity field

Measurements of the terminal velocity for the three HASE solutions are presented in Fig. 3. There is a critical volume V_c for which a velocity discontinuity appears. The value of this critical volume decreases with an increase in HASE concentration. These results are in agreement with those obtained by Herrera-Velarde *et al.*[10] In all cases, the

III. THEORY FOR SPHERICAL BUBBLES

A brief summary of the theory for Newtonian flow around spherical bubbles is presented. In general, the motion of a gas bubble is mainly determined by the hydrodynamic conditions (properties of the liquid, diameter of the bubble) and by the boundary condition on the bubble surface.

At very low Reynolds numbers (creeping flow), the flow is dominated by viscous effects. The equations of motion can, in principle, be solved rigorously and hence the drag can be calculated. By equating the drag and the buoyancy, the velocity-volume relationship can be obtained. The interface of a gas bubble may be considered between the two extreme cases of a free and a rigid interface.[26,27] If the gas is assumed to be inviscid, the tangential stress τ is zero at the free interface. For a rigid interface, the velocity of the interface is equal to the velocity of the center of gravity of the bubble. In other words, the no-slip boundary condition holds at the bubble surface. For either case, the drag force on a spherical bubble in creeping flow can be calculated[28–31] according to

slope of the velocity-volume relation is larger for large bubbles (for $V > V_c$) than for small bubbles (for $V < V_c$). Moreover, for a given volume, the terminal velocity decreases with an increase of HASE concentration (due to the increase of viscosity). It is important to observe that the increase in velocity after the discontinuity is significantly lower than that reported previously for aqueous shear-thinning viscoelastic liquids.[10,13] A distinctive feature of the discontinuity of the velocity-volume relation, for the HASE solutions, is that the slope of the curve, defined by dU/dV (where U is the velocity and V is the volume), increases significantly past the critical volume. Clearly, the value of dU/dV at the discontinuity is larger than the values corresponding for the nonjump condition (Table III). Moreover, the amplitude of the discontinuity decreases as the percentage of HASE increases.

Flow visualization around bubbles before and after the discontinuity using the PIV technique are presented in Figs. 4 and 5. For air bubbles with volumes smaller than the criti-

TABLE III. Velocity increase, dU/dV, at the volume for which the discontinuity occurs. dU/dV_{Hadamard} and dU/dV_{Stokes} are calculated from Eqs. (1) and (2).

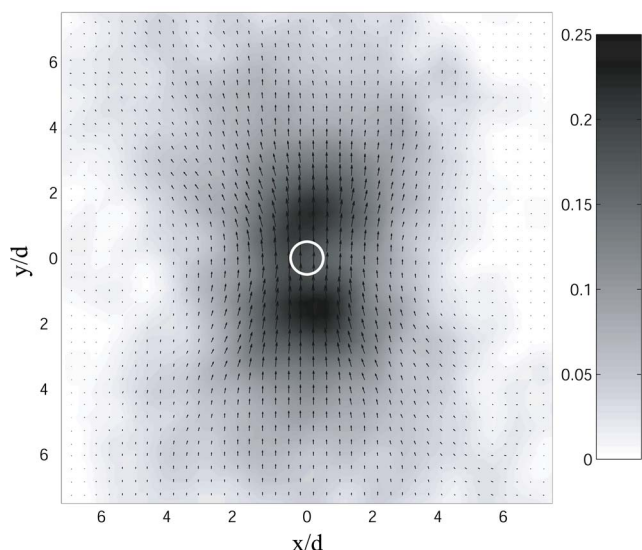| % HASE	dU/dV	dU/dV_{Hadamard}	dU/dV_{Stokes}
1.2%	2.52	0.43	0.28
1.5%	0.55	0.14	0.09
1.7%	0.188	0.06	0.04

FIG. 4. Flow around a rising bubble with volume below the critical one ($V=4.2$ mm³; $U=1.1$ mm s⁻¹; HASE 1.5%).

cal one, V_c, the fluid at the front and at the rear of the bubble is moving in the same direction of the bubble (Fig. 4). For bubbles with a volume larger than the critical one, V_c, the flow around the bubble is drastically different (Fig. 5). The flow at the front of the bubble is in the same direction of the bubble motion. At the rear of the bubble, the fluid is moving in the opposite direction of the bubble motion. This phenomenon is called negative wake and was previously reported elsewhere[3,11,32,33], and more recently in Ref. 10. The negative wake is a manifestation of importance of the elastic effects in the bubble motion. Presumably, the elasticity of the liquid is an important factor for the discontinuity to appear. This argument will be further discussed later.

B. Bubble shape

The velocity discontinuity can be related to the bubble shape. Figures 6–8 show bubbles for the three solutions with volumes smaller and larger than the critical one V_c. Clearly, there is a very significant change of the shape related to the appearance of the velocity jump.

For bubbles with a volume much smaller than the critical volume V_c, the shape is nearly spherical. With a small increase in volume, a slight deformation on the rear part of the bubble is observed. In all cases, for volumes smaller than V_c, the shape of the bubbles is convex all around, whereas for bubbles with a volume larger than the critical volume V_c, the shape is concave in the trailing end: the shape presents an inflection point. Figure 9 shows a comparison of the shape of a bubble before and after the jump. The shape in the front region is nearly the same, whereas it changes significantly in the back region. Moreover, the formation of a sharp cusp can be clearly observed. At the tip of the cusp, a long (few centimeters) and very thin (tens of micrometers) tail forms in all cases. Using two cameras acting simultaneously, it was possible to obtain a view of the tail from two sides. The cusps and tails immediately after V_c are axisymmetric. However, for volumes larger than V_c, this is no longer the case. Non-axisymmetric tails are shown and discussed in Sec. VII.

V. COMPARISON OF EXPERIMENTS AND THEORY FOR SMALL BUBBLES: TERMINAL VELOCITY

The viscosity of the HASE solutions displays a Newtonian region at small shear rates $\dot\gamma$. For small Reynolds numbers, one can attempt to compare the measured terminal velocities with those predicted for the Stokes-Hadamard drag [Eqs. (1) and (2)].

Figure 10 shows a comparison of experimental results obtained for fluid 1 (1.2% HASE). The predictions [Eqs. (1) and (2)] consider the measured zero shear-rate viscosity.
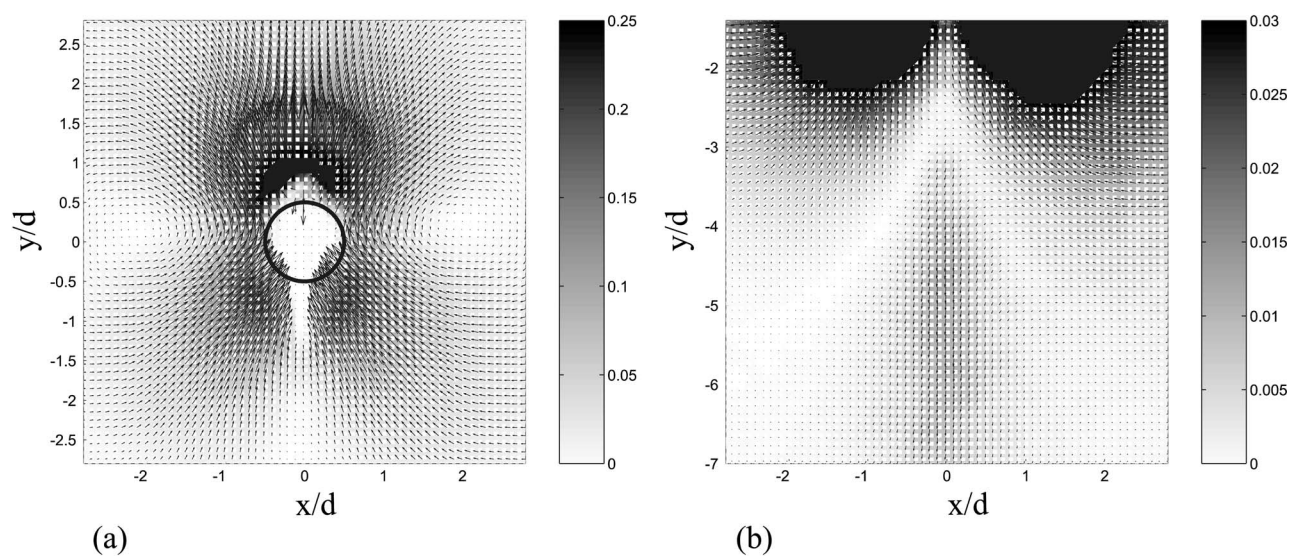

FIG. 5. Flow around a rising bubble with volume above the critical one. (a) Flow around the bubble. The flow is very similar to the flow observed for a bubble with a volume smaller than V_c. (b) At the rear part of the bubble, the negative wake can be seen ($V=239$ mm³; $U=54.6$ mm s⁻¹; HASE 1.5%).

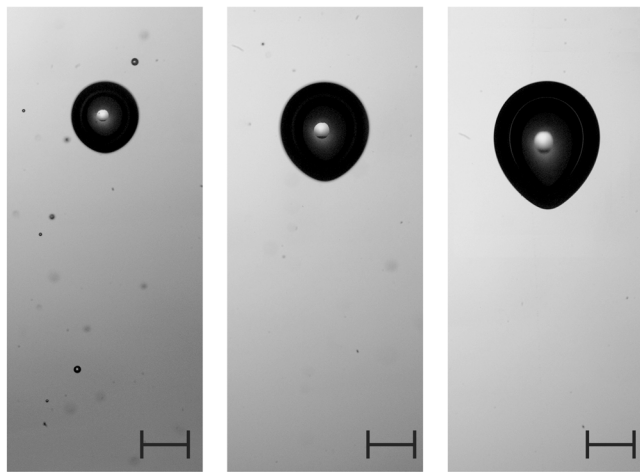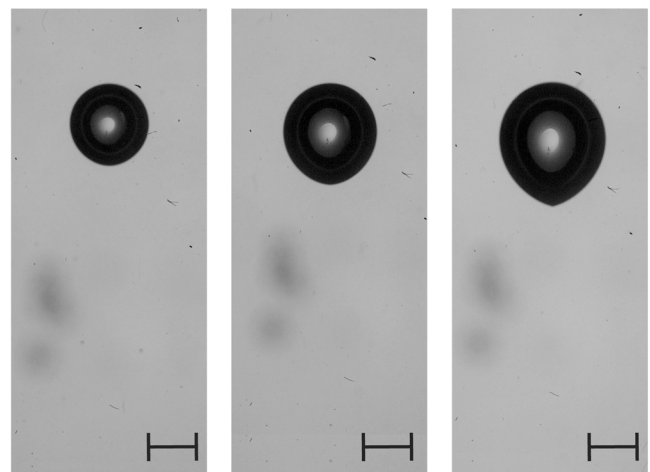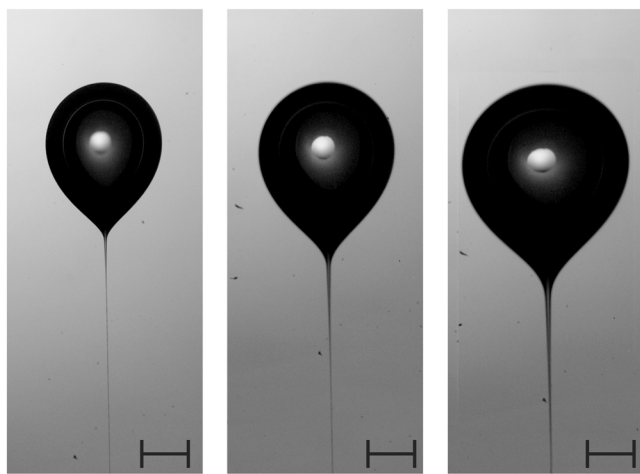V*=0.19   V*=0.46   V*=0.76

V*=1.04   V*=1.67   V*=2.94
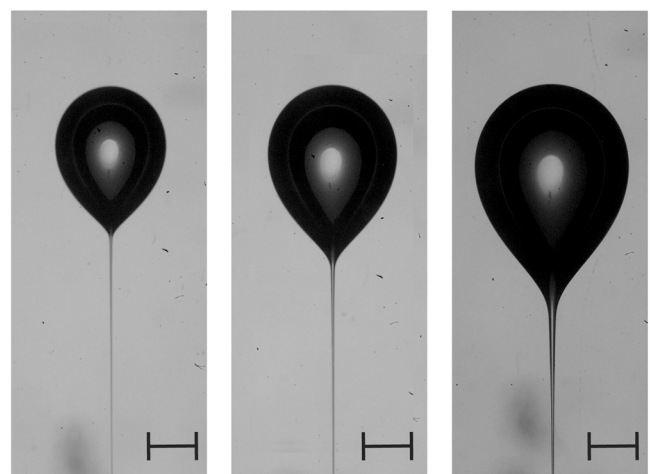
FIG. 6. Bubble shapes for different values of the dimensionless volume $V^*=V/V_c$ for %HASE=1.2, with $V_c=65$ mm^3. The small bubbles are almost spherical. For larger volumes (for $V^*>1$), the shape of the bubbles is concave with a very thin and long tail at the rear part of the bubble. The scale represents 2 mm.

V*=0.32   V*=0.55   V*=0.82

V*=1.02   V*=1.56   V*=2.66

FIG. 7. Bubble shapes for different values of the dimensionless volume $V^*=V/V_c$ for %HASE=1.5, with $V_c=60$ mm^3. The scale represents 2 mm.

Clearly, the disagreement among the two sets of data is apparent. The rheometric flow (simple shear), in which the viscosity was measured, contrasts that of the flow around the bubble. To improve the predictions, the viscosity of the liquid was obtained from a simple falling-bead setup. The effective viscosity in this case inferred from

$$\mu = \frac{2}{9}\frac{r^2 \Delta \rho g}{U},$$

where r is the bead radius (m), $\Delta\rho = \rho_{bead} - \rho_{liquid}$ is the density difference between bead and liquid (kg m^{-3}), g is the gravitational constant ($g=9.81$ m s^{-2}), and U is the terminal settling velocity of the sphere m s^{-1}.

The experiments are conducted by varying the diameter of the glass beads from 3 to 6 mm. In all the cases, the Reynolds number is smaller than 1. The shear rate is also small, corresponding to shear rates within the Newtonian re-

gion of the rheometric flow curve. In addition, the ratio d_s/D is smaller than 0.07 (d_s is the diameter of the bead and D is the diameter of the test section). The viscosity obtained from these experiments is constant for shear rates between 0.2 and 10 s^{-1}. The results are presented in Table IV. The viscosity obtained from falling-bead experiments is in all cases larger than that obtained under simple shear. The ratio of these viscosities (α) as a function of HASE percentage is shown in Table IV. This ratio decreases with HASE concentration. This behavior can be explained by two reasons.

First, in these experiments, wall effects are present. For Newtonian fluids, the drag correction factor reduces to the well-known Faxén correction,[35] which is commonly expressed in the form

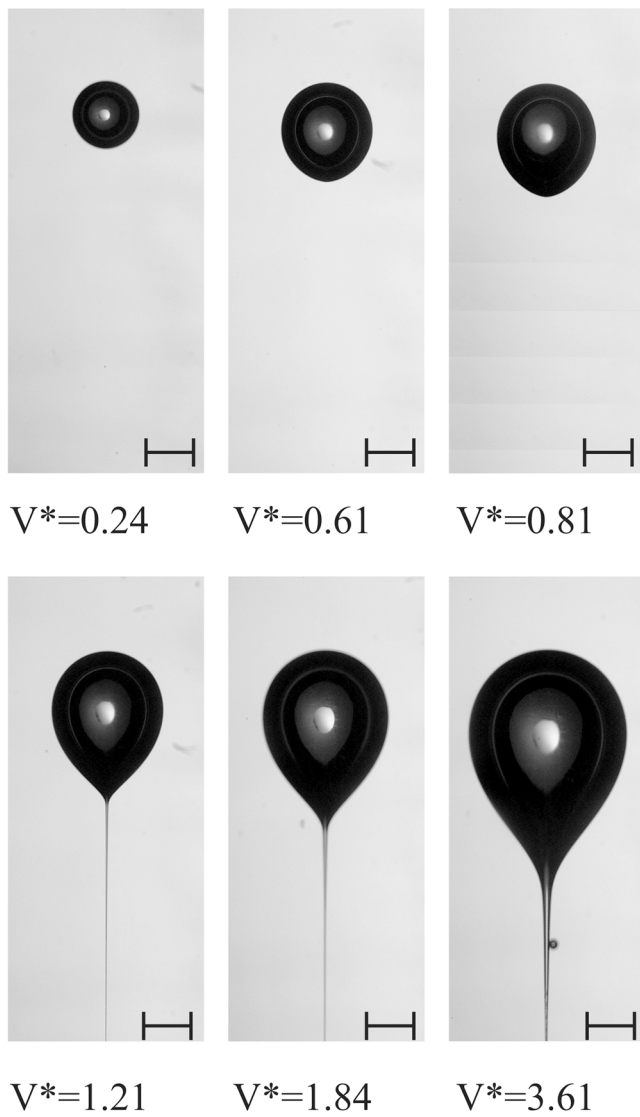$$K_N(a/R) = \frac{1}{1-f(r/R)} = \frac{U_{\text{Stokes}}}{U} \qquad (3)$$

with

V*=0.24   V*=0.61   V*=0.81

V*=1.21   V*=1.84   V*=3.61

FIG. 8. Bubble shapes for different values of the dimensionless volume $V^* = V/V_c$ for %HASE=1.7, with $V_c = 50$ mm^3. The scale represents 2 mm.
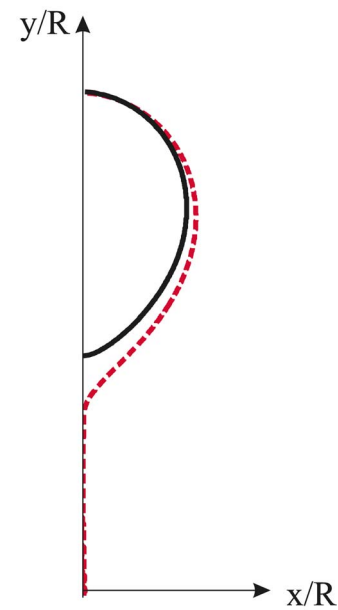

FIG. 9. Bubble shapes before (continuous line) and after (dashed line) the jump. The shape does not change in the front part of the bubble, whereas it changes in its back part (V_{before}=49.2 mm^3; V_{after}=61.2 mm^3; 1.5% HASE).

$$f(r/R) = 2.104\ 44(r/R) - 2.088\ 77(r/R)^3$$
$$+ 0.948\ 13(r/R)^5 + 1.372(r/R)^6 - 3.87(r/R)^8$$
$$+ 4.19(r/R)^{10} + \cdots, \tag{4}$$

where r is the radius of the falling bead and R is the container radius. This relation is only valid in the case of a Newtonian fluid for Reynolds number smaller than 1. It has been shown[36] that "for moderate Deborah Numbers De, wall effects appear to be less important than in the motion of the corresponding Newtonian fluid." In our experiments, the Deborah number lies between 0.5 and 1.6, implying that the drag correction factor is smaller than the one calculated in the case of a Newtonian fluid.[37] In these HASE solutions, a r/R value of 0.07 corresponds to $K_N(r/R) = 1.16$. It implies a viscosity increase of 1.16. Moreover, the wall correction factor for elastic, constant-viscosity fluids[38] is given by $f(r/R) = 1 - 0.17r/R$ for Deborah numbers larger than 0.2, which corresponds in our case to $K_N(r/R) = 1.006$. The wall effect contributes to a small increase in viscosity obtained from

falling-bead experiments over that obtained in simple shear. However, the difference between the two viscosities is within a factor of 2.

The second reason is that, conceptually, the flow around a bubble can be divided into three regions: a simple shear region at the equator, a simple extensional region at the rear, and a biaxial extensional region at the front. The extensional components lead to extra stresses that slow the sphere motion down. But this extensional flow depends on the Reynolds number. For large values of the Reynolds number the extensional components will be more important; as a consequence, the difference between the two viscosities will increase.

The ratio of the viscosity estimated from falling-bead data to the viscometric viscosity decreases with HASE concentration (Table IV). In addition to the wall effects, which decrease the terminal velocity and hence increase the viscosity, it is necessary to include the extensional flow contributions. Under extensional flow, models[17,18,39] predict a region of extensional thickening at extension rates of the order of the inverse of the main relaxation time. This region coincides with the onset for measurable normal stresses in shear flow, closely related to the appearance of the velocity discontinuity. The extensional flow contribution further retards the motion of the falling bead, increasing the mentioned viscosity ratio.

The experimental and theoretical results obtained with the two viscosity measurements are compared. The results are presented in Fig. 10. For small bubbles that are almost spherical, the experimental measurements lie between the two limiting cases of Hadamard and Stokes laws with a viscosity calculated from the falling-bead experiments. Therefore, the bubble interface can neither be considered fully contaminated nor clean. We note that the comparison is good for bubbles with volumes smaller than the critical volume V_c.
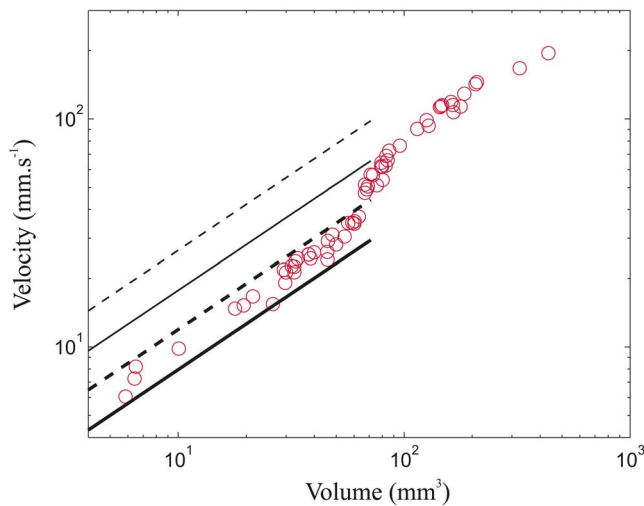
FIG. 10. Bubble velocity as a function of bubble volume, 1.2% HASE. The lines are the theoretical predictions obtained from the Stokes (continuous lines) and Hadamard (dashed lines) laws: (thin lines) $\mu = \mu_{\text{rheometer}}$; (thick lines) $\mu = \mu_{\text{fall}}$.
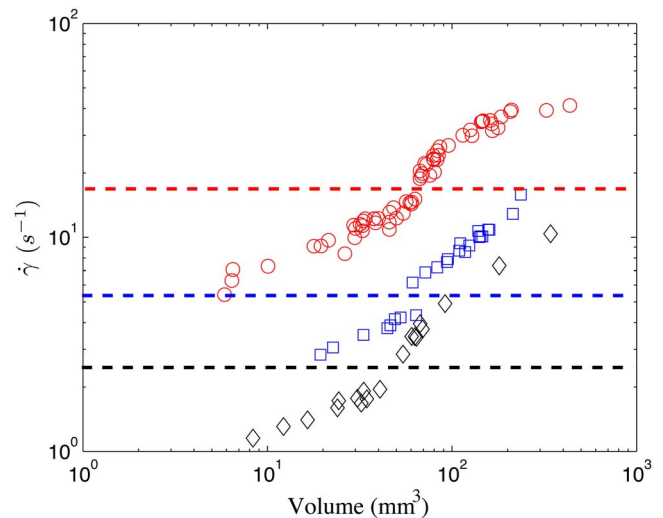

FIG. 11. Mean shear rates $\bar{\dot{\gamma}}$ as a function of the volume for different percentages of HASE: ○ 1.2%; □ 1.5%; ◇ 1.7%. The dashed lines represent, for each percentage of HASE, the shear rate for which the normal stresses are measurable.

Above V_c, the bubbles are no longer spheroidal and develop a long tail. The results for the other fluids and their comparison with the theory are not presented here, but the agreement between theory and experiments is equally good. Contrary to the measurement of the viscosity by falling-bead experiments, the simple shear rheological measurements do not take into account the uniaxial and biaxial deformations. This explains why the behavior of small bubbles rising in a viscoelastic fluid is better described using a falling-sphere measurement of the viscosity.

VI. INTERPRETATION

In the case of bubbles rising in an associative polymer, it has been shown that there is a critical value of the volume at which a discontinuity in the velocity-volume curve occurs. The analysis of the bubble shape shows that for small bubbles (with a volume smaller than the critical value), the shapes of the bubbles are convex: the bubbles are spherical or spheroidal. For volumes larger than the critical value, the shape of the bubbles is completely different: the bubbles are concave, there is an inflection point, and a very thin, long tail appears at the rear part of the bubble. Moreover, the velocity field around the bubbles also changes significantly for experiments below and above the critical volume. In particular,

for bubbles with volumes above the critical value, the presence of the so-called negative wake can be observed.

It is possible to link this behavior with the rheological properties of the fluid. For this, the mean shear rate (defined as $\bar{\dot{\gamma}} = U/r$) at which the normal stresses are measurable and at which the discontinuity of the velocity occurs, is determined. Figure 11 shows the calculated $\bar{\dot{\gamma}}$ for the three tested liquids. From this plot, the value of the shear rate corresponding to the critical volume can be determined and is approximately the same as the shear rate at which the elastic nature of the fluid begins to manifest itself (N_1 becomes measurable). Therefore, it can be said that the bubble velocity discontinuity is a direct result of the appearance of elastic stresses.

For negligible normal stresses, the bubbles are almost spherical and their velocities are governed by the Stokes and Hadamard laws. For significant normal stresses, the velocity is larger than the velocity predicted by Stokes and Hadamard law, and the bubbles are concave, presenting a tail at their rear part.

The immediate consequence of the presence of normal stresses in the liquid is a change in the bubble shape, which evidently leads to a drag reduction and, hence, a rapid increase of velocity. A particular bubble shape is then related to its rising velocity.

We have shown before that the elasticity of the liquid plays an important role, because the discontinuity of the velocity occurs when the normal stress appears in the liquid. Consequently, we can consider that the Deborah number, defined by the ratio of the first normal stress difference N_1 and two times the tangential stress $\tau = \mu \dot{\gamma}$, can be considered to determine when the discontinuity occurs;

TABLE IV. Viscosity measurements for different solutions with two methods: $\mu_{\text{rheometer}}$ is the viscosity measured in a cone-plane rheometer under simple shear, μ_{fall} is the viscosity calculated from falling-bead experiments. The ratio of the viscosity α decreases with increasing HASE concentration.

Fluid $n°$	% HASE	$\mu_{\text{rheometer}}$ (Pa s)	μ_{fall} (Pa s)	Viscosity ratio α
1	1.2	0.22	0.49±0.01	2.23
2	1.5	1.14	1.58±0.04	1.39
3	1.7	3.34	4.08±0.23	1.22
4 (Ref. 34)	2.1	12.5	13.23±0.4	1.06

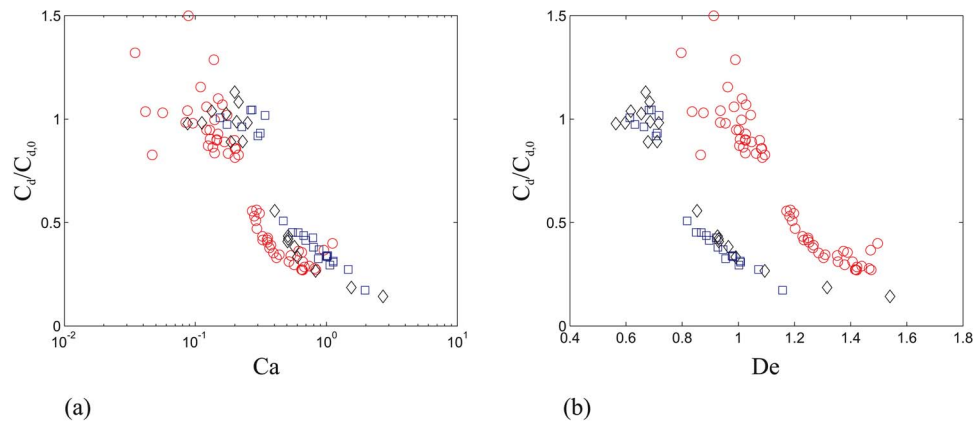$$\text{De} = \frac{N_1}{2\tau} = \frac{N_1 d}{4 \mu U}.$$

FIG. 12. (a) $C_d/C_{d,0}$ as a function of the Capillary number, (b) $C_d/C_{d,0}$ as a function of the Deborah number, for different percentages of HASE: ($\circ$) 1.2% HASE; ($\square$) 1.5% HASE; ($\diamond$) 1.7% HASE. The critical value of these dimensionless numbers for which the discontinuity of the velocity occurs depends on the percentage of HASE.

Since there is a strong change of the shape of the bubble before and after the discontinuity, this implies that the surface tension will also play an important role. Since the discontinuity of the velocity occurs for Reynolds number smaller than 1, the capillary number, defined by the ratio of the viscous forces and the surface forces, $Ca = \mu U/\sigma$ can also be considered to be an important parameter to the problem. We can define a normalized drag coefficient, which is equal to $C_d/C_{d,0}$, where $C_{d,0}$ is the Hadamard drag coefficient ($C_{d,0} = 16/Re$). For small bubbles (with a volume smaller than the critical one), the normalized drag coefficient will be close to 1. For large bubbles, there is an increase of the velocity. And so, for a decrease of the drag coefficient, the normalized drag coefficient will be smaller than 1. The normalized drag coefficient is shown in Fig. 12 as a function of the two dimensionless numbers previously defined. Clearly, for small De, the bubbles are spherical and $C_d/C_{d,0}$ is around 1. After a certain critical De, the normalized drag coefficient decays abruptly, corresponding to the point for which the discontinuity occurs. This behavior can be observed in the

three solutions. However, the value of the critical De for which the discontinuity occurs is not unique, as it depends on the percentage of HASE. A similar trend can be observed for the capillary number: at a critical value of Ca, the normalized drag drops abruptly, but this critical value is different for each liquid. Hence, neither De nor Ca can be used to capture a generally valid condition for the jump to occur. There are two main conclusions from the results of this analysis: (1) the discontinuity appears when the elastic properties manifest themselves and (2) there is a significant change in the shape associated with the bubble velocity increase. It is then appropriate to form a dimensionless group that compares elastic forces to capillary forces,

$$\Pi = \frac{N_1 d}{\sigma}.$$

This number would be large if elastic effects dominate over surface tension effects and vice versa. In fact, this number could be interpreted as $\Pi = 4Ca \times De$.

Figure 13 shows the normalized drag coefficient as a function of the dimensionless group Π. For this case, the transition from high to low drag appears to be the same for all the liquids: there is a critical value of Π ($\Pi_{crit} \simeq 0.25$) that determines the conditions for the bubble velocity discontinuity to appear for all the liquids tested.

The tail at the rear part of the bubble leads to a decrease of the drag coefficient and consequently to a rapid increase of the velocity. Since the tail shape can also influence the flow behavior of the bubble, the tail shape can be related to the bubble velocity. This aspect is further discussed in the next section.

VII. SHAPES OF THE TAILS

Lastly, we present a photographic study of the peculiar shapes of the bubble tails that appear after the bubble velocity discontinuity. Previously, it was observed that a long, thin axisymmetric tail appears on the rear part of bubbles immediately after the critical volume [this case is shown in Fig. 14(a)]. The thickness of the tail can be of the order of a few microns, while its length amounts to a few centimeters. The
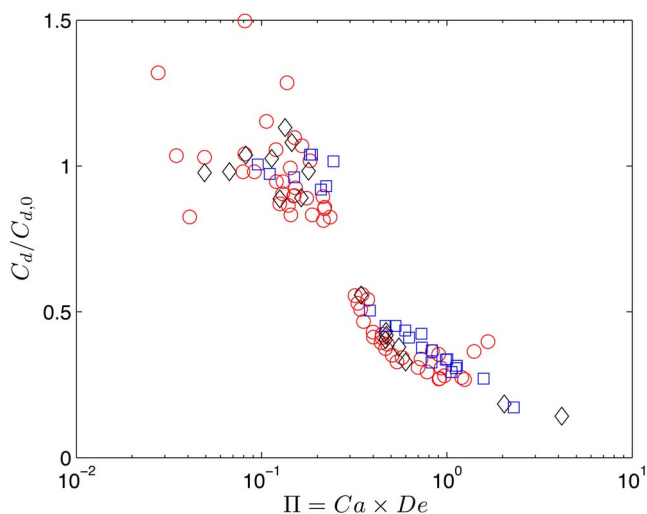

FIG. 13. Normalized drag coefficient as a function of $\Pi = Ca \times De$ for: ($\circ$) 1.2% HASE; ($\square$) 1.5% HASE; ($\diamond$) 1.7% HASE. For all the percentages of HASE, the discontinuity occurs for the same value of Π ($\Pi \simeq 0.25$).
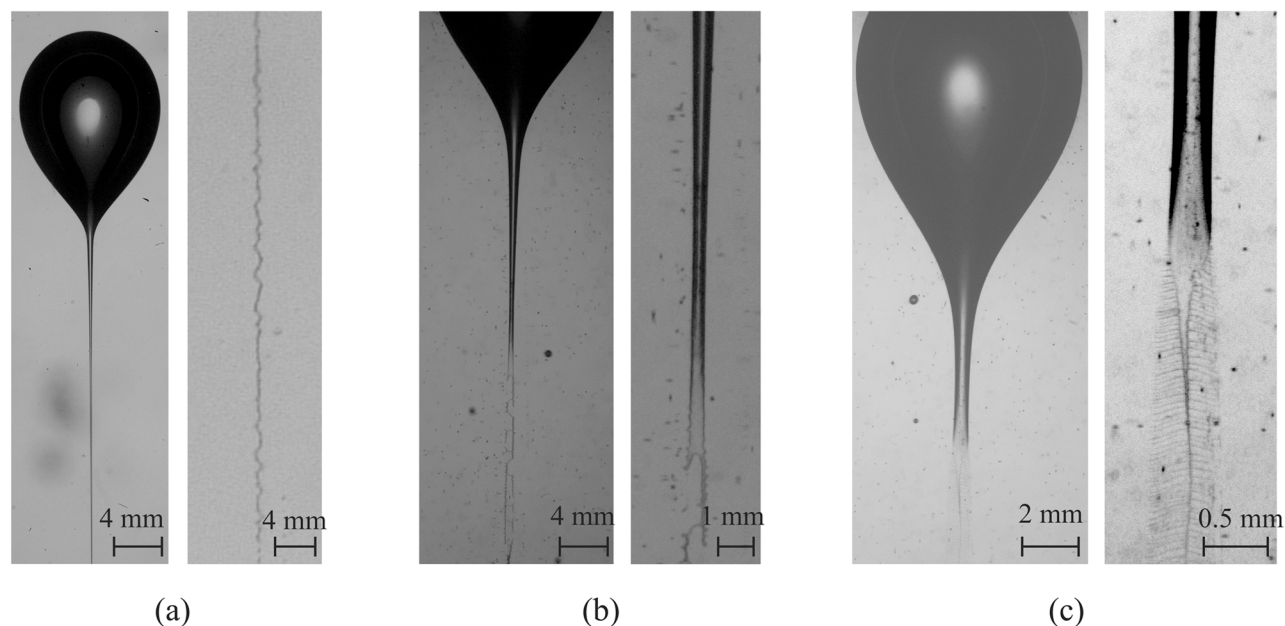
FIG. 14. Two perpendicular views (a) and (b) of the tail; the tail breaks into two different threads ($V=824$ mm^3, 1.5% HASE).

tail eventually breaks into micron-sized bubbles. This behavior resembles the so-called tip-streaming phenomena, when daughter drops are ejected from a thin thread at the tip of a highly stretched drop. The tip-streaming behavior was first reported by Taylor[40] and since then has been studied by many authors. To our knowledge, tip streaming has not been reported to date for the case of air bubbles moving in complex non-Newtonian liquids.

For larger bubble sizes, the cusped tip transforms into a "blade-edge" tip [two–dimensional (2D) cusp] [Figs. 14(b) and 14(c)]. The 2D cusped end was observed from simultaneous tail images taken at perpendicular views. Several experiments are necessary to obtain images in which the edge of the tail is parallel to the photo plane [images shown in Figs. 14(b) and 14(c)]. The appearance of such shapes has also been previously observed.[14] The 2D cusp does not have a preferential orientation. Note that these experiments are performed in a cylindrical tank.

Moreover, the streaming behavior can also be observed in 2D cusps; the so-called "edge streaming." We have observed that the 2D cusped tail can break into different manners for the same nominal experimental conditions. In some cases, the tail breaks into two different threads [Figs. 14(b) and 15]. The two threads extend for some distance, but eventually each one breaks into microbubbles. In some other cases, the 2D tails collapse into a single thread with perpendicular filaments that resemble a "fish backbone" [Figs. 14(c) and 16]. All these fine threads eventually break into small bubbles. Edge streaming has also not been previously reported for these fluids.

Clearly, the viscoelastic nature of the HASE solutions is responsible for the formation of the cusped and edged tips at the back of the air bubbles. However, the basic mechanism for the cusp-to-edge transition is not known. Tip streaming phenomenon is an indication that, near the cusp, high levels of fluid stretching are present. There is also a possibility that

the surface active ingredients are being convected along the bubble surface, inducing surface tension gradients, hence, enhancing the tip streaming.

To further investigate the conditions for which the 2D cusps appear, additional series of experiments were performed for such large bubbles. The terminal velocities were measured for increasing bubble volumes, and the shape of the tails was also identified. Figure 17 shows the terminal velocity of bubbles as a function of volume. The symbols denote different tail shapes observed experimentally. With the present experimental setup, it is difficult to determine precisely the critical volume from which the tail changes
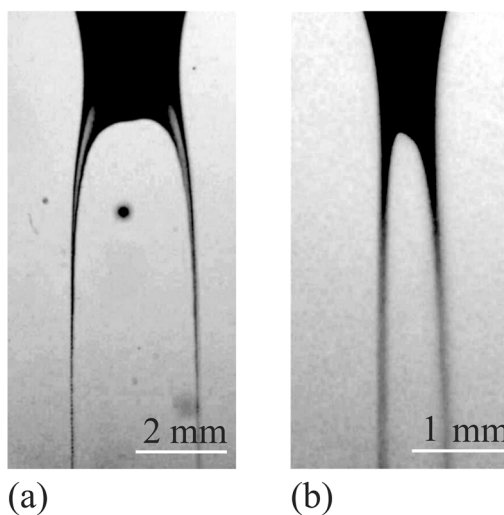

FIG. 15. Various tail shapes for bubbles moving in a 1.5% solution of HASE: (a) tip streaming: bubble with filament tail and zoom of the tail instability; (b) edge streaming: bubble with knife-edge tail and breakdown process of the tail edge; (c) edge streaming: bubble with knife-edge tail [the volume is larger than that shown in (b)] and breakdown process of the tail edge.
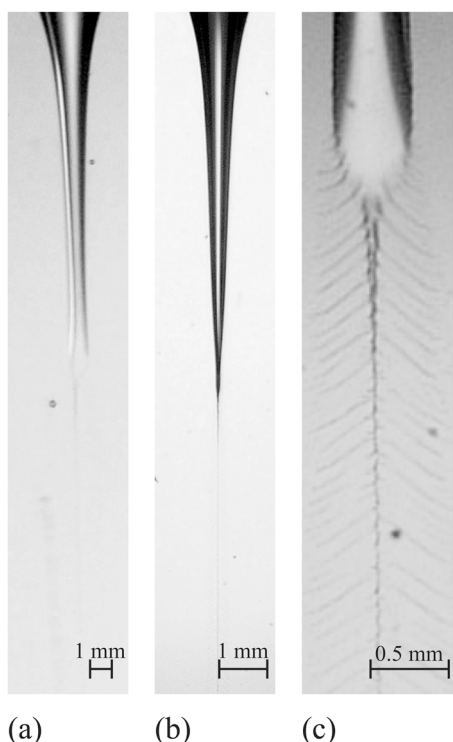
FIG. 16. Two perpendicular views (a) and (b) of the tail. (c) The tail collapses into a single thread with perpendicular filaments that resemble a "fish backbone" (V=391 mm^3, 1.5% HASE).

from axisymmetric to two dimensional (either two threaded or fish backbone).

For volumes smaller than 280 mm^3 (corresponding to shear rates smaller than 15 s^{-1}), the tail is axisymmetric, very thin, and long. For larger volumes, the 2D cusp appears. For volumes between 280 and 350 mm^3 (corresponding to shear rates between 15 and 18 s^{-1}), only fish-bone streaming is observed. For volumes larger than 350 mm^3 (corresponding to shear rates larger than 18 s^{-1}) both two-thread and
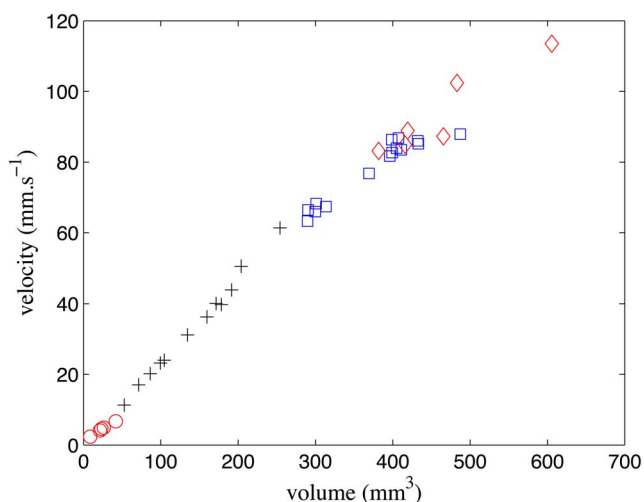

FIG. 17. Velocity as a function of the bubble volume for 1.5% HASE. Different critical values of the volume for the different bubble shapes: (∘) spheroidal bubbles; (+) axisymmetric tail (tip streaming); (□) 2D edged tail (fish-bone streaming); (◇) 2D edged tail (two-thread streaming).

fish-bone formations can be observed. Although the influence of the type of 2D tail on the terminal velocity of the bubble (drag coefficient) is not significant, we observed that when the two types of edge-streaming appear, a larger scatter of data of bubble velocity is observed.

The different shapes of tails reported in this section have never been observed for rising bubbles in either polymeric or worm-like micellar fluids. The formation of these different shapes may be, in fact, a result of the specific properties of the associative polymer fluid. Clearly, further experiments are needed to understand the formation process of a particular tail shape.

VIII. SUMMARY AND CONCLUSIONS

We have shown that for bubbles rising in an associative polymer solution, as the bubble volume increases, a discontinuity of the velocity occurs. This discontinuity in the velocity is smaller than that observed for aqueous shear-thinning viscoelastic liquids. A more distinctive feature for this case is that the slope of the relation velocity-volume increases significantly past the discontinuity. This particular behavior was studied for various HASE concentrations. It was possible to relate this discontinuity with the rheological properties of the fluid. In fact, the shear rates for which the discontinuity occurs correspond to those for which the normal stresses appear. It is important to note that the critical shear rates also correspond to the point at which the shear thickening appears in some solutions, which may contribute to reducing the strength of the velocity jump.

The discontinuity can also be related to the bubble shape and to the flow around the bubble. For volumes smaller than the critical volume, the bubbles are spherical or spheroidal and the flow around the bubble is similar to that of a Newtonian liquid. For volumes larger than the critical one, the rear of the bubble is concave and presents a tail at their rear part. The flow around the bubble is more complex, and the presence of a negative wake can be observed.

This study provides a criterion for the determination of a critical volume. Due to the importance of the elasticity and the surface tension, a dimensionless number defined as $\Pi = N_1 d/\sigma$ is proposed to determine the jump conditions. The discontinuity occurs for $\Pi_{crit} \simeq 0.25$.

For the case of small bubbles, we found good agreement between experiments and predictions for the velocities according Stokes-Hadamard laws. For small bubbles, the shear rate is small, and consequently, the liquid can be considered as Newtonian. For this agreement, the viscosity had to be obtained with a falling-bead technique. In agreement with previous investigations, we found that the viscosity determined in this manner was larger than that obtained under simple-shear viscometric flow.

For large bubble volumes, we presented a photographic study of the bubble shapes and particularly the tail shapes. Different kinds of tails can be observed.

From the present results, we have determined that the appearance of the discontinuity results from a balance between elastic and surface tension forces. We are currently conducting additional experiments with other non-

Newtonian liquids (Boger, inelastic, etc.) to further corroborate the appropriateness of the Π group to describe the conditions of the bubble velocity discontinuity. These results will be reported in a future communication.

ACKNOWLEDGMENTS

[1] R. Clift, J. R. Grace, and M. E. Weber, *Bubbles, Drops and Particles* (Academic, New York, 1978).

[2] R. P. Chhabra, *Bubbles, Drops and Particles in Non-Newtonian Fluids* (CRC, Boca Raton, FL, 1993).

[3] D. Funfschilling and H. Z. Li, "Flow of non-Newtonian fluids around bubbles: PIV measurements and birefringence visualisation," Chem. Eng. Sci. **56**, 137 (2001).

[4] G. Astarita and G. Apuzzo, "Motion of gas bubbles in non-Newtonian liquids," AIChE J. **11**, 815 (1965).

[5] S. M. Barnett, A. E. Humphrey, and M. Litt, "Bubble motion and mass transfer in non-Newtonian fluid," AIChE J. **12**, 253 (1966).

[6] P. H. Calderbank, D. S. Johnson, and J. Loudon, "Velocity fields around spheres and bubbles investigated by laser-Doppler anemometry," Chem. Eng. Sci. **25**, 235 (1970).

[7] L. G. Leal, J. Skoog, and A. Acrivos, "On the motion of gas bubbles in a viscoelastic fluid," Can. J. Chem. Eng. **49**, 569 (1971).

[8] D. Rodrigue, D. De Kee, and C. F. Chan Man Fong, "Bubble velocities: further developments on the jump discontinuity," J. Non-Newtonian Fluid Mech. **79**, 45 (1998).

[9] D. Rodrigue, D. De Kee, and C. F. Chan Man Fong, "An experimental study of the effect of surfactants on the free rise velocity of gas bubbles," J. Non-Newtonian Fluid Mech. **66**, 213 (1996).

[10] J. R. Herrera-Velarde, R. Zenit, D. Chehata, and B. Mena, "The flow of non-Newtonian fluids around bubbles and its connection to the jump discontinuity," J. Non-Newtonian Fluid Mech. **111**, 199 (2003).

[11] O. Hassagar, "Negative wake behind bubbles in non-Newtonian liquids," Nature **279**, 402 (1979).

[12] M. T. Arigo and G. H. McKinley, "An experimental investigation of negative wakes behind spheres settling in a shear-thinning viscoelastic fluid," Rheol. Acta **37**, 307 (1998).

[13] E. Zana and L. G. Leal, "The dynamics and dissolution of gas bubbles in a viscoelastic fluid," Int. J. Multiphase Flow **4**, 237 (1978).

[14] Y. J. Liu, T. Y. Liao, and D. D. Joseph, "A two-dimensional cusp at the trailing edge of an air bubble rising in a viscoelastic liquid," J. Fluid Mech. **304**, 321 (1995).

[15] M. A. Winnik and A. Yekta, "Associative polymers in aqueous solution," Curr. Opin. Colloid Interface Sci. **2**, 424 (1997).

[16] K. C. Tam, L. Guo, R. D. Jenkins, and D. R. Bassett, "Viscoelastic properties of hydrophobically modified alkali-soluble emulsion in salt solutions," Polymer **40**, 6369 (1999).

[17] O. Manero, F. Bautista, J. F. A. Soltero, and J. E. Puig, "Dynamics of worm-like micelles: the Cox-Merz rule," J. Non-Newtonian Fluid Mech. **106**, 1 (2002).

[18] F. Bautista, J. M. de Santos, J. E. Puig, and O. Manero, "Understanding thixotropic and antithixotropic behaviour of viscoelastic micellar solutions and liquid crystalline dispersions. I. The model," J. Non-Newtonian Fluid Mech. **80**, 93 (1999).

[19] A. Belmonte, "Self oscillations of a cusped bubble rising through a micellar solution," Rheol. Acta **39**, 554 (2000).

[20] S. Chen and J. P. Rothstein, "Flow of a wormlike micelle solution past a falling sphere," J. Non-Newtonian Fluid Mech. **116**, 205 (2004).

[21] A. Jayaraman and A. Belmonte, "Oscillations of a solid sphere falling through a wormlike micellar fluid," Phys. Rev. E **67**, 065301(R) (2003).

[22] A. M. Mollinger, E. C. Cornelissen, and B. H. A. A. van den Brule, "An unexpected phenomenon observed in particle settling: oscillating falling spheres," J. Non-Newtonian Fluid Mech. **86**, 389 (1999).

[23] P. H. T. Uhlherr, T. N. Le, and C. Tiu, "Characterisation of inelastic power-law fluids using falling sphere data," Can. J. Chem. Eng. **54**, 497 (1976).

[24] D. Rodrigue (private communication).

[25] Y. Caram, F. Bautista, J. E. Puig, and O. Manero, "On the rheological modeling of associative polymer," Rheol. Acta (to be published).

[26] D. Hammerton and F. H. Garner, "Gas absorption from single bubbles," Trans. Inst. Chem. Eng. **32**, S18 (1954).

[27] V. G. Levich, *Physico-Chemical Hydrodynamics* (Prentice-Hall, Englewood Cliffs, NJ, 1962).

[28] G. G. Stokes, *Mathematical and Physical Papers* (Cambridge University Press, England, 1880).

[29] H. Schlichting, *Boundary Layer Theory* (McGraw-Hill, New York, 1964).

[30] J. Hadamard, "Mouvement permanent lent d'une sphere liquide et visqueuse dans un liquide visqueux," C. R. Acad. Sci. Paris **152**, 1735 (1911).

[31] W. Rybczynski, "Uber die Fortschreitende Bwegung einer-ussigen Kugel in einem zahen Medium," Bull. Acad. Sci. Cracovie Ser. A **1**, 40 (1911).

[32] C. Bisgaard and O. Hassager, "An experimental investigation of velocity fields around spheres and bubbles moving in non-Newtonian liquids," Rheol. Acta **21**, 537 (1982).

[33] H. Z. Li, X. Frank, D. Funfschilling, and Y. Mouline, "Towards the understanding of bubble interactions and coalescence in non-Newtonian fluids: a cognitive approach," Chem. Eng. Sci. **56**, 6419 (2001).

[34] A. Mendoza Fuentes, "Diseño, construccion y aplicacion de un equipo de asentamiento de particulas en un polimero asociativo," Master thesis, Universidad Nacional Autonoma de Mexico, 2006.

[35] J. Happel and H. Brenner, *Low Reynolds Number Hydrodynamics* (Prentice-Hall, Englewood Cliffs, NJ, 1973).

[36] G. H. McKinley, *Transport Processes in Bubbles, Drops and Particles*, edited by R. Chhabra and D. DeKee (Taylor and Francis, New York, 2002), Chap. 14.

[37] R. P. Chhabra, C. Tiu, and P. H. T. Uhlherr, "A study of wall effects on the motion of a sphere in viscoelastic fluids," Can. J. Chem. Eng. **59**, 771 (1981).

[38] R. P. Chhabra and P. H. T. Uhlherr, "The influence of fluid elasticity on wall effects for creeping sphere motion in cylindrical tubes," Can. J. Chem. Eng. **66**, 154 (1988).

[39] E. S. Boek, J. T. Padding, V. J. Anderson, P. M. J. Tardy, J. P. Crawshaw, and J. R. A. Pearson, "Constitutive equations for extensional flow of wormlike micelles: Stability analysis of the Bautista-Manero model," J. Non-Newtonian Fluid Mech. **126**, 39 (2005).

[40] T. D. Taylor and A. Acrivos, "On the deformation and drag of a falling viscous drop at low Reynolds number," J. Fluid Mech. **18**, 466 (1964).